JOURNAL OF MATERIALS SCIENCE 17 (1982) 2809–2816

Structure dependence of thermally induced microcracking in porcelain studied by acoustic emission

G. KIRCHHOFF, W. POMPE, H.-A. BAHR
Zentralinstitut für Festkörperphysik und Werkstofforschung, Akademie der Wissenschaften der DDR zu Berlin, Dresden, DDR

In porcelain during cooling the smaller thermal expansion coefficient of the glassy phase compared with the quartz particles causes radial tensile stresses and may create microcracks between these two components. The initiation and growth of microcracks due to thermal stresses has been studied by applying the acoustic emission technique. Different sources of microcracks are detected depending on thermal history. The acoustic emission spectrum is approximately a superposition of two maxima near the phase transition of quartz and cristobalite. Microcracking depends on particle size. With decreasing size of the quartz particles the maximum of microcrack activity shifts to lower temperatures.

1. Introduction

The optimization of the structure by controlled technologies yields a remarkable increase of the strength of porcelain [1–6]. In this connection thermal stresses caused by an α–β phase transition of quartz and the thermal mismatch between the components of porcelain play an important role [7–9]. The smaller thermal expansion coefficient of the glassy phase compared with the quartz particles gives rise to radial tensile stress during cooling and may create microcracks between these two components [10–13].

The efficiency of the acoustic emission technique for the detection of microcracks arising under applied load in ceramics has been demonstrated by many authors [14–16]. This paper deals with initiation and growth of microcracks due to thermal stress. In connection with this, the different sources of microcracking will be discussed, depending on thermal history and the influence of structural parameters, especially the size of the quartz particles.

2. Experimental technique

2.1. Heating arrangement

In general, acoustic emission transducers cannot be used at high temperatures. Therefore several workers in this field have described their special apparatus for receiving the acoustic signals of heated specimens [17–20]. For our purposes thermal shock loading [19] is not suitable. The application of the other techniques leads to difficulties with respect to reproducibility of the acoustic coupling between specimen, wave guide and transducer. Unwanted variations of the measuring sensitivity with temperature cannot be avoided. Therefore an arrangement with inhomogeneous temperature distribution along the rod-shaped porcelain specimen was used (Fig. 1). The centre of the specimen was placed in a small furnace, where it could be thermally loaded according to schedule. Due to the low thermal conductivity of porcelain, the ends of the rod were nearly at room temperature and the acoustic transducer could easily be coupled by means of vacuum grease. In this way the porcelain rod served as a specimen and as a wave guide at the same time. By fastening the rod at one end outside the furnace, thermally induced axial stress as well as frictional noise from displacements between specimen and furnace were absent. The heating and cooling schedule was realized by temperature control. The temperature was measured by a thermocouple.

0022–2461/82/102809–08$03.46/0

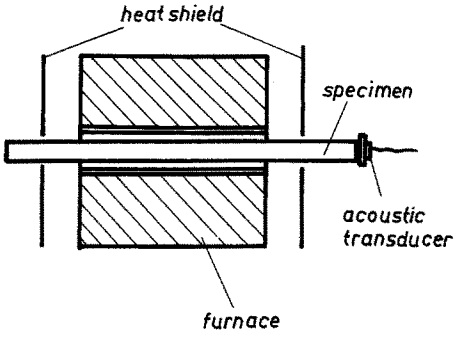

Figure 1 Heating arrangement for acoustic emission investigations.

2.2. Acoustic emission equipment

The acoustic emission equipment consisted of a piezoelectric transducer (resonant frequency at about 240 kHz), a commercial low-noise preamplifier, frequency filter, main amplifier, and the signal processing electronics. The applicable detecting sensitivity for emission signals was equivalent to a trigger level of 1.5 μV at the transducer output. The signal processing electronics provided standard pulses for ring-down and event counting. Emission rates and temperature were recorded with a three-pen-recorder as well as on punched tape [21]. In some of the experiments the pulse length of each signal was electronically measured and analysed [22].

3. Temperature dependence of microcracking

All measurements were done on fired samples of 150 mm length and 10 mm diameter. At first it was shown by means of a special test programme that our thermal cycle did not cause macroscopic cracking. The cycle consisted of heating at a rate of 700 K h^{-1} and subsequent cooling to room temperature at the same rate. The typical acoustic emission of a cycle is shown in Fig. 2 (note the change of scale). There is low emission at heating with a small maximum at 520 K due to the α-β transition of cristobalite. On cooling, however, the emission is more than 100 times stronger. It is mainly confined to the region below 920 K with a large peak between 670 and 770 K. In the following, we will consider the emission at cooling only.

Characteristic circumferential microcracks around the quartz particles were detected in all samples (Fig. 3). This led to the assumption that extensive microcracking might be the source of the measured high emission rates. The circumferential structure indicated that cracking was governed by radial tensile stress.

In order to assess the amount of internal stress, a self-consistent model for the thermal mismatch was made use of. As a structural element we used a composite sphere consisting of an inner quartz sphere surrounded by a thin cristobalite layer and a glassy matrix shell. These elements are embedded in a so-called effective material, the constants of which are the very macroscopic observables that are to be derived from the model under the condition of self-consistency. The model leads to a three-dimensional thermoelastic boundary problem, which has been solved [23].

The physical properties of the crystalline phases were approximated by isotropic material constants. The temperature dependence of elastic constants and thermal expansion of quartz and cristobalite was fitted to experimental data by Salmang [24]. The sudden changes which these parameters undergo near phase transition points were also included in this model. The unknown temperature dependence of thermal expansion of the glassy

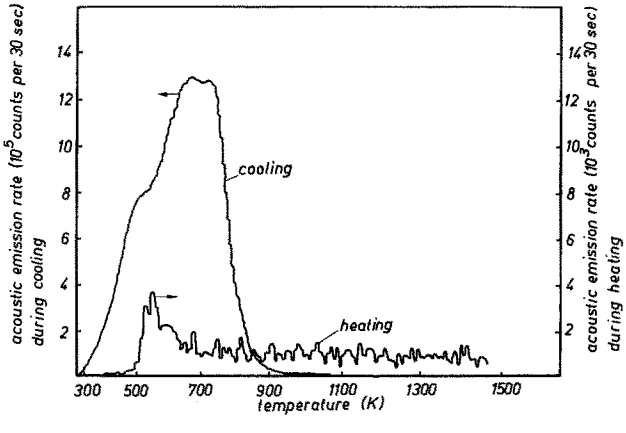

Figure 2 Temperature dependence of acoustic emission during heating and cooling of porcelain.

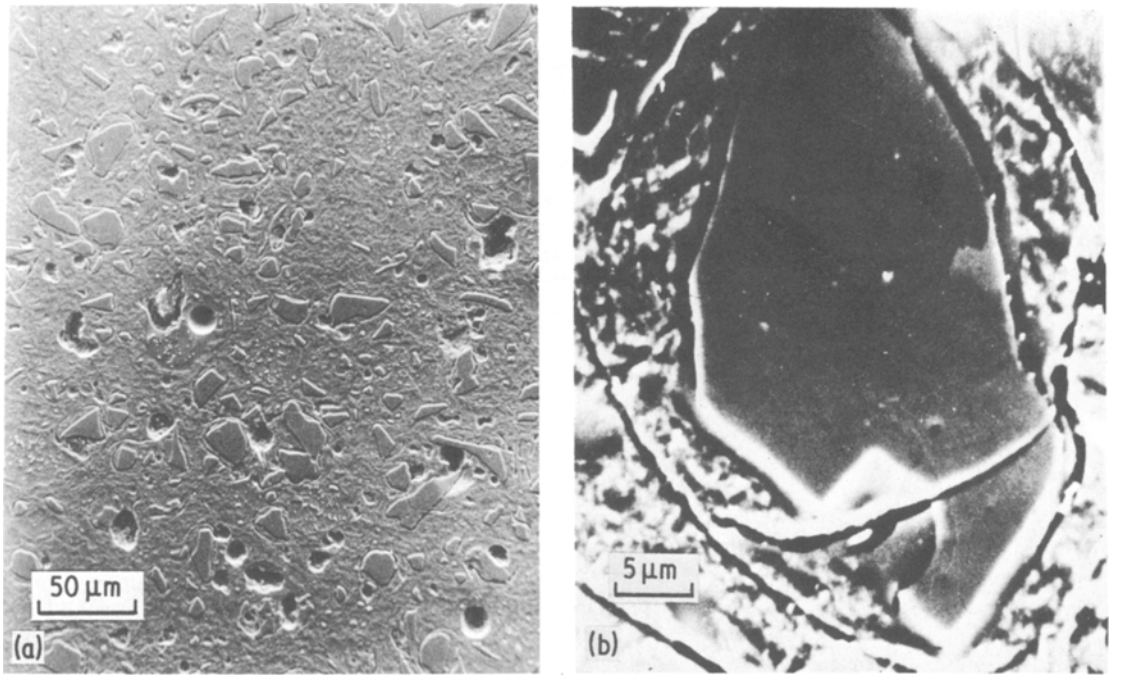

Figure 3 Scanning electron micrograph of porcelain showing typical circumferential cracks around large quartz particles.

matrix was fitted to that of the porcelain by comparing experimental data with the relation that has been derived theoretically from this model. In this way the internal stresses within the components were calculated by successive incremental changes of the temperature. In doing so one does not know, however, at which temperature the stress-free state should be assumed. Creep tests indicate an onset of flow at temperatures above 1100 K, whereas at 1300 K extensive viscous flow can be observed. The theoretical curves of Fig. 4 were calculated assuming the sample to be stress-free at 1270 K. This assumption, of course, is to some degree arbitrary.

Our theoretical results (Fig. 4) show that radial tensile stress arises only during cooling below 840 K, which is the transition point of quartz, and increases all the way down to room temperature. Therefore microcracking can only occur below 840 K, which is in accordance with the emission measurements.

In order to obtain more detailed information about the mechanisms at work in porcelain during cooling, a special series of experiments with the same temperature schedule as described above but with systematically increased maximum temperature T_{max} was performed.

When heating up to no more than 770 K, only weak emission rates were observed at cooling, with a maximum at about 470 K. After heating to higher temperatures $T_{max} > 920$ K the emission at cooling was higher. In addition to the known emission peak at about 470 K corresponding to the transition of cristobalite, a second, very intense peak appeared at about 840 K (Fig. 5), being related to the phase transition of quartz.

At cooling from still higher temperatures,

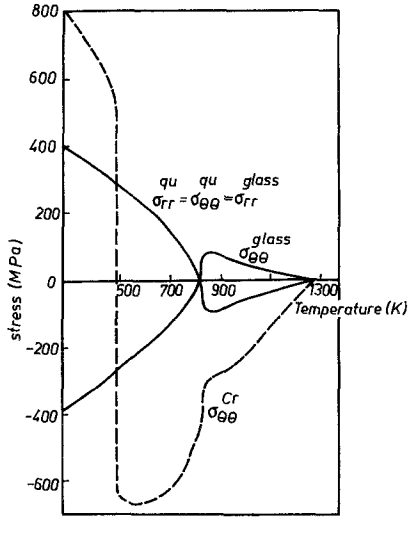

Figure 4 Temperature dependence of the maximal radial and tangential stresses, σ_{rr} and $\sigma_{\theta\theta}$, respectively, in a composite sphere of quartz (qu) particles surrounded by a thin cristobalite (cr) layer in a glassy (glass) matrix.

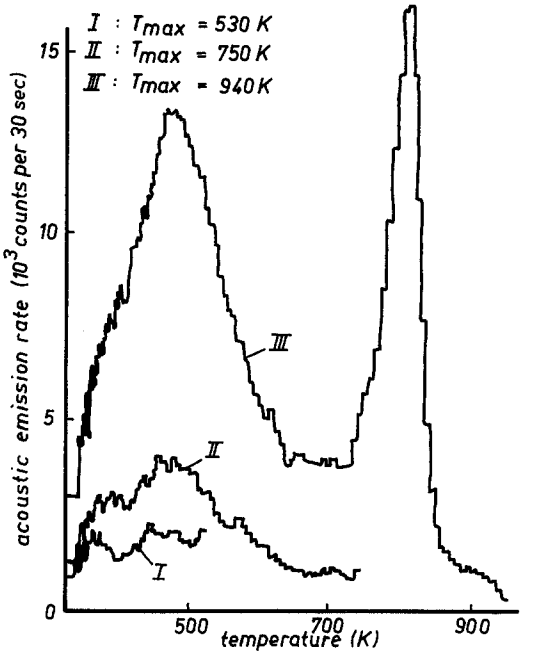

Figure 5 Temperature dependence of acoustic emission during cooling of porcelain.

we found a third mechanism being activated, which becomes predominant for $T_{max} > 1270\,K$. Then the two maxima at 470 K and 840 K merged into one (Fig. 6). The predominant peak just mentioned is supposedly caused by mircocracking as discussed above. The interesting behaviour observed in this experimental series, namely

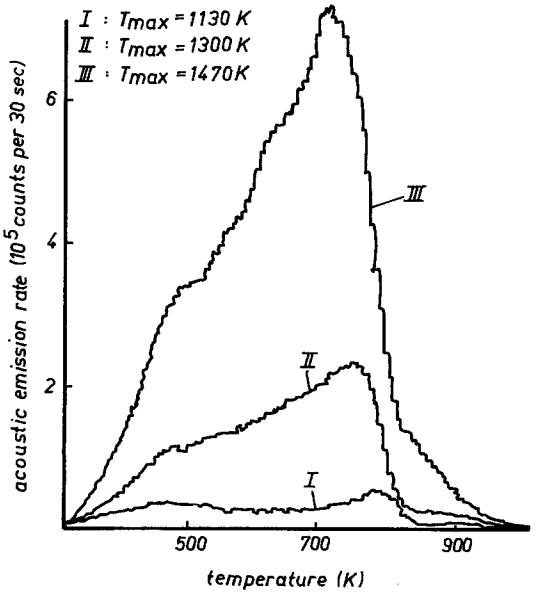

Figure 6 Temperature dependence of acoustic emission during cooling of porcelain.

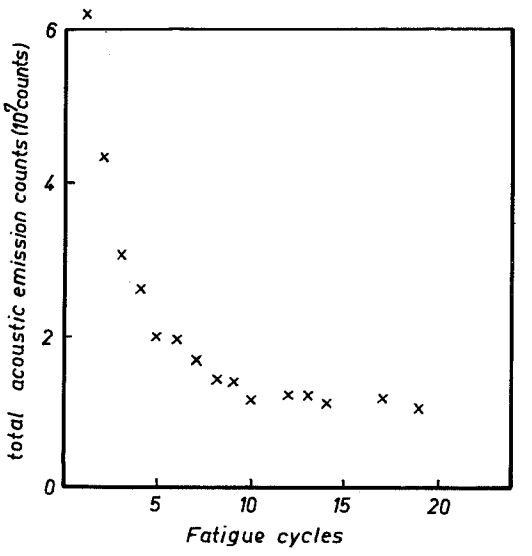

Figure 7 Total acoustic emission plotted against load cycle during thermal loading of porcelain.

the strong dependence of microcracking on the maximum temperature of the cycle, can be explained by stress relaxation in the glassy matrix below 1100 K during the period of heating. Assuming the existence of circumferential microcracks at room temperature (Fig. 3), during heating the quartz particles expand more than the glassy matrix, and the existing cracks will close. Above 840 K the crack surfaces are pressed together (Fig. 4). As soon as the transformation range of the glassy matrix is reached, the cracks start healing. The beginning of microcrack healing was observed at $T_{max} \approx 1130\,K$ (Fig. 6), which agrees well with the known transformation range of the matrix from 1070 K to 1170 K. In order to investigate the extent of healing, one specimen was repeatedly heated to 1470 K and cooled. The sum of acoustic emission counts of one cycle systematically decreased from cycle to cycle (Fig. 7). This shows that even during heating up to 1470 K the microcracks do not heal completely, and that after about 20 cycles the ability of healing is nearly exhausted.

4. Particle size dependence of microcracking.

From ceramics literature it is well known that microcrack initiation depends significantly on the size of grains or inclusions (see, for instance [25–29]). Polycrystalline materials with grains or inclusions smaller than a critical size do not microcrack, whereas those with larger grain

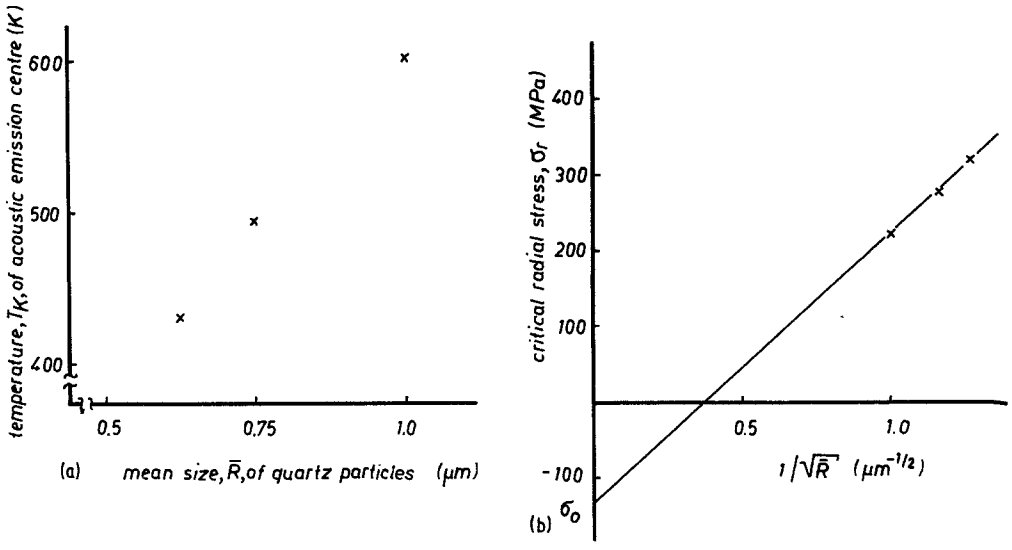

Figure 8 Dependence of microcracking on the size of quartz particles during cooling of porcelain. (a) Critical temperatures from acoustic emission data. (b) Critical radial stresses determined from (a) using Fig. 4.

sizes do. Thermally induced microcracking of porcelain also shows a particle-size dependence of this kind (Fig. 3).

We investigated the size effect for three types of porcelain. Depending on the special technology of sintering, the mean diameters of the quartz particles were 1.25 μm, 1.5 μm and 1 μm. Each kind of porcelain had a definite particle-size distribution from less than 0.5 μm to about 10 μm. The emission spectra of these kinds of porcelain show, at constant cooling rate, a significant effect due to the silica grain size. The acoustic emission centre for the cooling rate of 700 K h^{-1} shifted to lower temperatures with decreasing particle size (Fig. 8a).

Furthermore, the size dependence of the amplitude spectrum was determined. For this purpose the acoustic pulses were classified with respect to pulse width into 10 equidistant channels. Corresponding to the given particle size distribution of a given sample, different emission activities were observed at the different pulse-width channels. In Fig. 9a the temperature T_K of the acoustic emission centre is plotted against

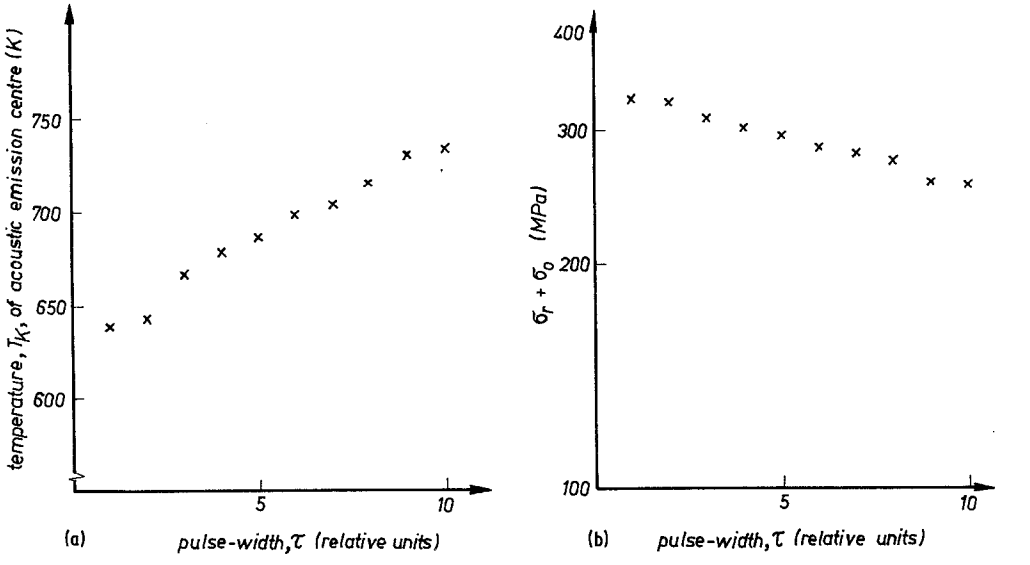

Figure 9 Dependence of microcracking on the energy of acoustic emission signals. (a) Critical temperatures plotted against width of emission signals. (b) Critical radial stresses determined from (a) using Fig. 4.

number of pulse-width channel. As above, the cooling rate was $700\,K\,h^{-1}$.

Interpreting these size dependences we will confine ourselves to microcracking due to radial tensile stress near the surface of the quartz particles. That is, we consider crack propagation along that interface to be connected with acoustic emission near the α-β transformation of quartz. Let us follow an energy approach discussed by Lange [30]. The variation of the elastic strain energy with the crack area A can be described in the following manner

$$W_{el} = \eta R^3 f(x), \qquad x = \frac{A}{4\pi R^2}, \quad (1)$$

where R is the particle radius and ηR^3 the stored energy for vanishing crack area. For the following it is essential that the unknown function, $f(x)$ has an inflection [30]. Approximating the surface energy W_γ needed for crack extension by

$$W_\gamma = 2\gamma A, \quad (2)$$

the total energy

$$W = W_{el} + W_\gamma, \quad (3)$$

schematically shown in Fig. 10, shows a non-monotonic dependence on the normalized crack area x for not too small values of ηR. After [30], the maxima and minima correspond to conditions of crack extension and crack arrest, respectively, according to

$$\frac{dW}{dA} = 0, \qquad \frac{d^2W}{dA^2} < 0 \text{ crack extension;}$$

$$\frac{d^2W}{dA^2} > 0 \text{ crack arrest.} \quad (4)$$

Thus a generalized Griffith condition for crack extension follows from Condition 4 with the Equations 1, 2 and 3

$$\eta R = 8\pi\gamma \frac{1}{|f'(x_0)|}, \quad (5)$$

where x_0 means the normalized area of the pre-existing cracks and the prime denotes the derivative with respect to x.

Eliminating the total energy in Equation 1, Equation 3 can be written in the form

$$\frac{W}{4\pi\gamma R^2} = 2\left(\frac{f(x)}{|f'(x_0)|} + x\right). \quad (6)$$

This function is shown schematically in Fig. 10.

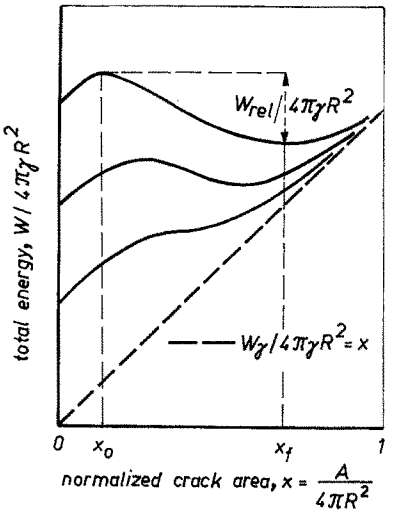

Figure 10 Schematic plot of the total energy against normalized crack area (analogous to Lange [30]).

Let us denote the energy detected by the acoustic emission equipment by W_{det}. This energy,

$$W_{det} \sim W_{rel}, \quad (7)$$

is assumed to be proportional to the energy W_{rel} released during propagation of a single microcrack in Fig. 10. In addition to this it is supposed that the propagating crack will be arrested at the final crack area x_f given by the minimum of the energy plot in Fig. 10 [30]. In doing so, inertial or stress wave reflection effects [31] are neglected during the crack propagation around the particle. After Fig. 10, W_{rel} is given by

$$W_{rel} = W(x_0) - W(x_f) = 8\pi\gamma R^2 F(x_0). \quad (8)$$

This function depends only on the normalized area of the pre-existing crack x_0, because the right-hand-side function in Equation 6, and consequently x_f, are determined by x_0 only. Turning back to the observed dependence on particle size R, let us consider the case where x_0 is independent on R. This corresponds to the assumption of an initial crack length being proportional to the particle size. This seems to have been justified for various ceramics by experiment (see for instance [28] and [29]). With this assumption it follows from Equation 5 and Equations 6, 7 and 8 that:

(a) the critical energy density for microcrack initiation decreases proportionally to $1/R$; and

(b) the detected energy increases proportionally to R^2. In order to substantiate the result (a), the radial stress has been plotted in Fig. 8b for the

different temperatures of maximal emission activity. In doing so we used the temperature dependence of stress from Fig. 4. The plot of Fig. 8b seems to support Equation 5 if we neglect a significant influence of the temperature dependence of the elastic moduli in this range of temperature, that is, if we assume

$$\eta \sim [\sigma_r(T) + \sigma_0]^2 \quad (9)$$

or

$$\sigma_r(T) \simeq cR^{-1/2} - \sigma_0. \quad (10)$$

Here c and σ_0 are constants, where σ_0 is the unknown temperature-independent contribution to the stress resulting from the uncertainty concerning the stress-free state. Comparing this relation with the experimental data, we obtain $\sigma_0 = 136$ MPa. This means that the stress-free state would be realized at about 900 K (Fig. 4).

Recently similar relations between critical internal stress and particle size were used in [26] and [27] in trying to explain the grain size dependence of microcrack initiation in brittle materials. Discussing non-cubic single-phase ceramics without phase transitions, the cited authors used a simpler approach to the thermal stress field. Unlike that and other publications, where microcracking was detected by non-linearities of the temperature dependence of the elastic moduli [32], thermal expansion [33], or thermal diffusivity [34], the acoustic emission technique provides a more direct possibility of microcrack detection.

Measuring the energy of the acoustic bursts offers additional information about the propagation of single microcracks. In Fig. 9b the logarithm of $\sigma_r + \sigma_0$ has been plotted versus acoustic pulse-width, τ. Keeping in mind that the pulse-width, τ, is related to the detected energy by

$$W_{det} \sim \exp c\tau, \quad (11)$$

this curve agrees with $\eta \sim W_{det}^{-1/2}$ following from the above results (a) and (b) and Equation 9 by elimination of the particle size, R. As yet it seems not quite reasonable, however, to compare quantitatively the slope of this curve with the theoretical result, because our apparatus allowed measurement of the relative pulse width only.

5. Conclusions

The acoustic emission technique offers additional insight into the temperature dependence of microcracking of porcelain. Summarizing the observations, the following can be stated:

(a) The maximum of microcracking is connected with high internal stress resulting from cooling. The overall acoustic emission is approximately a superposition of two maxima near the α-β phase transition of quartz (≈ 840 K) as well as the cristobalite transition (≈ 490 K).

(b) Microcracking depends on the thermal history. Microcrack healing of porcelain begins above 1120 K. The microcracks do not heal completely. Repeated thermal cycling up to 1470 K yields a stable final state after about 20 cycles.

(c) Microcracking depends on particle size. With decreasing size of the quartz particles the maximum of microcrack activity shifts to lower temperatures.

References

1. F. ZAPP, *Ber. Deut. Keram. Ges.* **42** (1965) 344.
2. A. MIELDS and C. ZOGRAFON, *ibid.* **44** (1967) 453.
3. G. N. MASLENNIKOWA, *Silikattechnik* **24** (1973) 304.
4. K. H. SCHÜLLER, *Ber. Deut. Keram. Ges.* **44** (1967) 212.
5. *Idem, ibid.* **44** (1967) 284.
6. *Idem, ibid.* **44** (1967) 387.
7. D. WEYL, *ibid.* **36** (1959) 319.
8. A. WINTERLING, *ibid.* **38** (1961) 9.
9. J. SELSING, *J. Amer. Ceram. Soc.* **44** (1961) 419.
10. K. H. SCHÜLLER and K. STARK, *Ber. Deut. Keram. Ges.* **44** (1967) 458.
11. D. B. BINNS, *Sci. Ceram.* **1** (1962) 315.
12. T. WIEDMANN, *Sprechs.* **92** (1959) 29.
13. P. SCHUSTER, Dissertation, Technische Universität Clausthal (1970).
14. J. J. SCHULDIES, *Mat. Eval.* **31** (1973) 209.
15. A. G. EVANS, M. LINZER and L. R. RUSSEL, *Mat. Sci Eng.* **15** (1974) 253.
16. A. G. EVANS, *J. Amer. Ceram. Soc.* **58** (1975) 239.
17. D. HUMS and D. JAX, *Sci. Ceram.* **7** (1973) 1.
18. G. C. ROBINSON, C. R. REESE and E. A. LaROCHE, Jr., *Ceram. Bull.* **53** (1974) 482.
19. A. G. EVANS, M. LINZER, H. JOHNSON, D. P. H. HASSELMAN and M. E. KIPP, *J. Mater. Sci.* **10** (1975) 1608.
20. H. SCHOLZE, D. POPESCU-HAS and H. SCHILLALIES, *Ber. Deut. Keram. Ges.* **53** (1976) 305.
21. G. KIRCHHOFF and H. SIX, *Feingerätetechnik* **28** (1979) 163.
22. H. SIX and G. KIRCHHOFF, Dissertation AdW der DDR, ZFW Dresden (1980).
23. W. POMPE, S. VÖLLMAR and W. KREHER, Tagung strukturabhängiges Verhalten von Festkörpern, Dresden, 11–13 October (1976).

24. H. SALMANG, "Die Keramik" (Springer, Berlin, 1958).
25. E. D. CASE, J. R. SMYTH and O. HUNTER, *J. Mater. Sci.* **15** (1980) 149.
26. R. W. RICE and R. C. PROHANKA, *J. Amer. Ceram. Soc.* **62** (1979) 559.
27. A. G. EVANS, *Acta Met.* **26** (1978) 1845.
28. D. R. CLARKE, *Acta Met.* **28** (1980) 913.
29. M. V. SWAIN, *J. Mater. Sci.* **16** (1981) 151.
30. F. F. LANGE in "Fracture Mechanics of Ceramics" Vol. 2, edited by R. C. Bradt, D. P. H. Hasselman and F. F. Lange, (Plenum, New Yrok, 1974) p. 599.
31. A. G. EVANS, *Proc. Brit. Ceram. Soc.* **25** (1975) 217.
32. R. R. SUCHOMEL and O. HUNTER Jr., *J. Amer. Ceram. Soc.* **59** (1976) 149.
33. O. D. SLAGLE, *Carbon* **7** (1969) 337.
34. H. J. SIEBENECK, D. P. H. HASSELMAN, J. J. CLEVELAND and R. C. BRADT, *J. Amer. Ceram. Soc.* **60** (1977) 336.

Received 22 October 1981
and accepted 1 February 1982